Article

Lack of support for surface diffusion of postsynaptic AMPARs in tuning synaptic transmission

Jary Y. Delgado[1],*
[1]Department of Biology, University of Chicago, Chicago, Illinois

ABSTRACT Repetitive stimulation of excitatory synapses triggers molecular events required for signal transfer across neuronal synapses. It has been hypothesized that one of these molecular events, the diffusion of extrasynaptic α-amino-3-hydroxy-5-methyl-4-isoxazolepropionic acid receptor (AMPARs) (i.e., the diffusion hypothesis), is necessary to help synapses recover from paired-pulse depression. To examine this presumed role of AMPAR diffusion during repetitive presynaptic stimulation, a biophysical model based on published physiological results was developed to track the localization and gating of each AMPAR. The model demonstrates that AMPAR gating in short intervals of fewer than 100 ms is controlled by their position in relation to the glutamate release site and by their recovery from desensitization, but it is negligibly influenced by their diffusion. Therefore, these simulations failed to demonstrate a role for AMPAR diffusion in helping synapses recover from paired-pulse depression.

SIGNIFICANCE Understanding the mechanisms regulating synaptic transmission is fundamental to understanding synaptic function, impacting current and future research. In this study, a biophysically realistic model of a glutamatergic synapse was used to examine the role of α-amino-3-hydroxy-5-methyl-4-isoxazolepropionic acid receptors (AMPARs) in synaptic transmission, as proposed by the diffusion hypothesis. This hypothesis proposes that synaptic AMPARs are replaced by mobile extrasynaptic AMPARs during periods of repetitive presynaptic stimulation. However, the model failed to demonstrate that extrasynaptic AMPARS replace synaptic AMPARs at rates sufficient to support the hypothesis. Therefore, the AMPAR diffusion hypothesis should be further reevaluated in future research.

INTRODUCTION

The response dynamics of excitatory synapses are regulated by pre- and postsynaptic factors (1,2). When presynaptic glutamate terminals are stimulated, calcium enters the cytosol and triggers fusion of glutamate-containing vesicles with the presynaptic plasma membrane (3). The probability of this event occurring, varies between synapses. During short intervals of paired presynaptic stimuli, below 200 ms, synapses display either paired-pulse depression (PPD) or paired-pulse facilitation. Whereas PPD is mostly controlled by presynaptic factors, the diffusion of postsynaptic α-amino-3-hydroxy-5-methyl-4-isoxazolepropionic acid receptor (AMPAR) has been shown to help synapses recover faster from PPD (hereafter referred to as the diffusion hypothesis) (4).

The AMPAR diffusion hypothesis states that synapses recover faster from PPD when postsynaptic AMPAR diffusion is allowed. It claims that, during paired-pulse stimulation, the first pulse of glutamate desensitizes synaptic AMPARs that are then replaced by nondesensitized extrasynaptic AMPARs. This frequently cited work, with over 400 citations, was supported by the following: 1) results from single-particle imaging experiments showing that AMPARs, when imaged using bulky red-shifted quantum dots, diffused rapidly on the plasma membrane and 2) the common understanding that a large pool of extrasynaptic AMPARs are present (5–9). However, we now have a better understanding of the synapse, and neither of these assumptions are true. For example, we now know the following: 1) there are very few extrasynaptic receptors (10–12), 2) extrasynaptic AMPARs do not move fast enough to replace the desensitized AMPARs at the synapse (10,13–16), 3) synapses contain a reduced pool of mobile receptors (13,15), and 4) intrasynaptic diffusion is confined to nanodomains and at orders of magnitude lower than previously thought (10,13,14,17).

This manuscript carefully examines the diffusion hypothesis by using a biophysical model of a glutamatergic synapse containing glutamate, glutamate transporters, AMPARs, and N-methyl D-aspartate receptors (NMDARs). This model incorporates the most recent findings, detailed in points 1–4 above, and contrasts the findings with the older ideas (4,18,19). The molecules are free to diffuse and interact based on experimentally derived realistic values. Contradicting the diffusion hypothesis, the model shows that most AMPARs do not diffuse fast enough to replace the desensitized synaptic AMPARs and, therefore, these findings do not validate the role of AMPAR diffusion during repetitive glutamatergic stimulation.

MATERIALS AND METHODS

Computer modeling was performed using the MCell and CellBlender simulation environment run on a laptop with an Intel Core i7-8650U Processor (Intel, Santa Clara CA) at 1.90 GHz 2.11 GHz with 16.0 GB of random access memory. A detailed description of the MCell/CellBlender simulation environment can be found in Gupta et al. (20).

AMPAR gating was simulated using the kinetic scheme published by Budisantoso et al. and described in Fig. 1 with the rate constants in Table 1 (21). Similarly, the gating scheme of NMDARs followed a modified scheme described by Lester and Jahr (22). R_o is the resting state, C1 and C2 are the two glutamate-bound closed states, O is the open state, and D is the desensitized state. In the model, the resting state was assigned the color blue and the open state assigned the color burgundy. The forward and backward rate constants are also given in Table 1.

Transporters cleared glutamate from the synapse following the kinetic scheme described by Gupta et al. (20). Free transporters were colored in deep blue and glutamate-bound transporters were colored in pink. T0 is the resting state, T1 and T2 are the two glutamate-bound states, and T0 is the state representing transport of glutamate across the plasma membrane. The rate constants are also described in Table 1.

Simulations were carried out with a time step of 0.1 ms for 1100 iterations (110 ms) or with a 1 μs time step (dt) for 5 ms. This dt was sufficiently short to maximize the precision and speed of the molecular events, given the available computer power.

The number of open and desensitized AMPARs were exported, and the values were plotted using GraphPad Prism 5.0 (GraphPad, San Diego, CA). When needed, statistical analyses were performed.

RESULTS

The biophysically realistic glutamatergic synapse was built using average values of a postsynaptic spine (24–26). The synapse consists of a postsynaptic spine, presynaptic area, and surrounding sheath (representing glia, axons, and other postsynaptic profiles present in the neuropil), which is separated from the pre- and postsynaptic profiles by 20 nm (Fig. 1 A) (24–26). The volume of the postsynaptic spine is 0.09 μm^3, with a postsynaptic diameter of 560 nm; the length of the neck is 0.6 μm, with a diameter of 110 nm, and a postsynaptic density (PSD) area of 0.08 μm^2. There is a 20 nm gap to represent the synaptic cleft.

Surface proteins were positioned (or released) at the PSD and at extrasynaptic areas, defined as the area away from the synaptic cleft. The initial model had 91 AMPARs placed within the PSD and a varied amount of extrasynaptic AMPARs, 25 NMDARs, and 100 other molecules representing obstacles to diffusion (e.g., neuroligin, cadherins, metabotropic glutamate receptors, K channels, etc.). This molecular density was extracted from the numbers of particles counted in the freeze-fractured image of a large CA1 postsynaptic spine reported by Shinohara and Hirase (11). The model also contained glutamate transporters at a density of 1000 molecules/μm^2, positioned on all surfaces but not within the synaptic cleft. Although this transporter density is low, it represents an average of the various glutamate transporters present at synapses (27–29). There were a total of 1130, 709, and 1380 glutamate transporters at the glia, presynaptic axon, and dendrites, respectively.

AMPAR gating was simulated using the kinetic scheme published by Budisantoso et al. (Fig. 2); the rates constant are described in Table 1 (21). The AMPAR kinetic states are color coded as follows: resting state (*green*), two glutamate-bound closed states (*yellow*), the desensitized states (*orange*, including a glutamate binding event), and open state (*white*). Like the AMPARs, the NMDARs also reacted with glutamate. The NMDAR gating scheme followed a modified scheme from Lester and Jahr (22); these kinetic states are also color coded: closed (*blue*) and opened
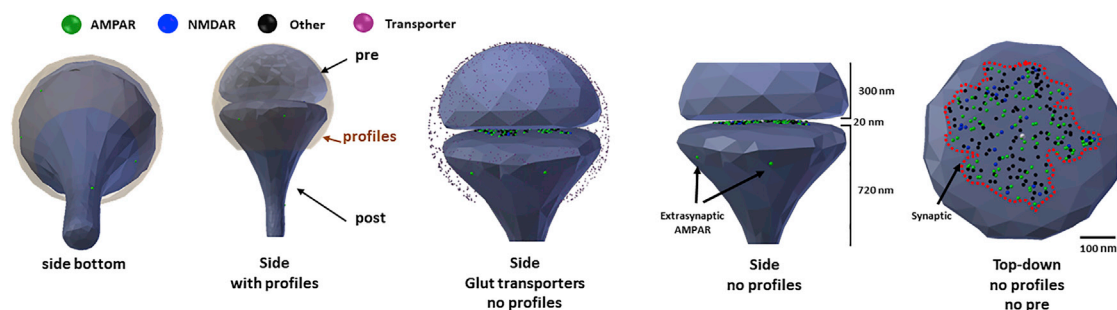

FIGURE 1 Anatomy of the CellBlender-based synapse. Views of the synapse from left to right. The first two views show synapse with all components. The third profile shows synapse with hidden synaptic profiles and transporters. The fourth profile zooms pre- and postsynapse, showing two extrasynaptic AMPARs in the postsynaptic spine. 300 nm size of presynaptic button and 720 nm size of postsynaptic spine are shown. The last profile shows a top-down view of the postsynaptic spine. Colored dots represent the resting AMPARs and NMDARs; in black are other synaptic proteins. The white dot is the center of the synapse and dashed line demarks the postsynaptic density. To see this figure in color, go online.
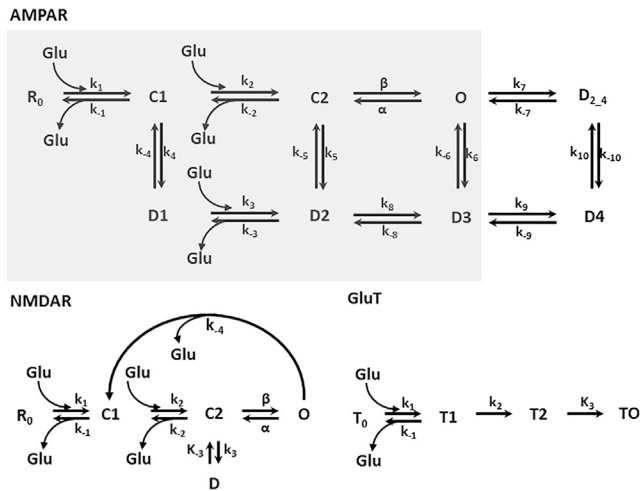
TABLE 1 Kinetic schemes for AMPAR, NMDAR, and glutamate transporter

		Forward		Backward	Reference
AMPAR					Budisantoso et al. (21)
	k_1	$13.66 \times 10^6 \ M^{-1} \ s^{-1}$	k_{-1}	$2.093 \times 10^3 \ s^{-1}$	
	k_2	$6.091 \times 10^6 \ M^{-1} \ s^{-1}$	k_{-2}	$4.719 \times 10^3 \ s^{-1}$	
	k_3	$13.66 \times 10^6 \ M^{-1} \ s^{-1}$	k_{-3}	$446.23 \ s^{-1}$	
	k_4	$1.00 \times 10^3 \ s^{-1}$	k_{-4}	$60 \ s^{-1}$	
	k_5	$1.8 \times 10^3 \ s^{-1}$	k_{-5}	$4.5 \ s^{-1}$	
	k_6	$12.36 \ s^{-1}$	k_{-6}	$1.5 \ s^{-1}$	
	k_7	$500 \ s^{-1}$	k_{-7}	$590.9 \ s^{-1}$	
	k_8	$40 \ s^{-1}$	k_{-8}	$420.9 \ s^{-1}$	
	k_9	$10.34 \times 10^3 \ s^{-1}$	k_{-9}	$140 \ s^{-1}$	
	k_{10}	$233.2 \ s^{-1}$	k_{-10}	$0.3242 \ s^{-1}$	
	β	$17.23 \times 10^3 \ s^{-1}$	A	$3.734 \times 10^3 \ s^{-1}$	
AMPAR (2)					Jonas et al. (23) and Heine et al. (4)
	k_1	$4.56 \times 10^6 \ M^{-1} \ s^{-1}$	k_{-1}	$4.26 \times 10^3 \ s^{-1}$	
	k_2	$2.84 \times 10^7 \ M^{-1} \ s^{-1}$	k_{-2}	$3.26 \times 10^3 \ s^{-1}$	
	k_3	$1.27 \times 10^6 \ M^{-1} \ s^{-1}$	k_{-3}	$45.7 \ s^{-1}$	
	k_4	$2.89 \times 10^3 \ s^{-1}$	k_{-4}	$39.2 \ s^{-1}$	
	k_5	$172 \ s^{-1}$	k_{-5}	$0.727 \ s^{-1}$	
	k_6	$17.7 \ s^{-1}$	k_{-6}	$4 \ s^{-1}$	
	k_8	$16.8 \ s^{-1}$	k_{-8}	$190 \ s^{-1}$	
	β	$900 \ s^{-1}$	A	$4.24 \times 10^3 \ s^{-1}$	
NMDAR					Lester and Jahr (22
	k_1	$1.7 \times 10^7 \ M^{-1} \ s^{-1}$	k_{-1}	$4.7 \ s^{-1}$	
	k_2	$5.6 \times 10^6 \ M^{-1} \ s^{-1}$	k_{-2}	$9.4 \ s^{-1}$	
	k_3	$8.4 \ s^{-1}$	k_{-3}	$1.8 \ s^{-1}$	
			k_{-4}	$9.4 \ s^{-1}$	
	β	$46.5 \ s^{-1}$	α	$91.6 \ s^{-1}$	
GluT					Gupta et al. (20)
	k_1	$1.8 \times 10^7 \ M^{-1} \ s^{-1}$	k_{-1}	$180 \ s^{-1}$	
	k_2	$180 \ s^{-1}$			
	k_3	$25.7 \ s^{-1}$			

(*purple*). The opening of the NMDAR requires two glutamate binding events (Fig. 2). Free glutamate transporters (color coded *pink*) clear glutamate from the synapse following the kinetic scheme described by Gupta et al. (20). The color of the kinetic states remains constant throughout the study only on figures showing the postsynaptic spine.

The binding and gating of AMPARs were assessed after the release of 4000 glutamate molecules into the synaptic cleft and compared with published results (24). Glutamate was released 15 nm away from the postsynaptic membrane and allowed to diffuse with a diffusion coefficient of $3.29 \times 10^6 \ cm^2/s$, as described by Diamond (30). First, the gating of a single AMPAR was evaluated. 13 μs after glutamate release, the AMPAR entered the open state (Fig. 3 A). The receptor remained open for 123 μs before entering the resting state, and as the glutamate diffused across the synaptic cleft, the receptor opened three more times and entered the first desensitized state after 761 μs. Next, the behavior of all AMPARs was recorded (Fig. 3, B and C). Release of 4000 glutamate molecules led to the gating of 91 AMPARs within 100 μs, as seen by Budisantoso et al. (21). Of these, 20 AMPARs (22%), those furthest away from the release site (>125 nm), were in the resting state (*green*), 16

AMPARs (18%) quickly entered the open state (*white*), 51 AMPARs (56%) were in the closed glutamate-bound state (*yellow*), and four AMPARs (4%) were desensitized (*brown*) (Fig. 3 C; Video S1). By 1000 μs after glutamate release, 32 AMPARs (35%) were in the resting state (*green*), 12 AMPARs (13%) were in the open state (*white*), 17 AMPARs (19%) were in the closed glutamate-bound state (*yellow*), and 26 AMPARs (or 29%) were desensitized (*brown*). A longer simulation was then performed and revealed similar results. As expected, glutamate release opened a comparable number of AMPARs, and within 10 ms after glutamate release, all AMPARs entered the closed state, whereas glutamate was still being transported away from the synapse. This was quantified as an increase in the amounts of [G][T], which represents the associated state between glutamate (G) and its transporter (T) (Fig. 4 A, *top and bottom*). Of note, the highest concentration of opened AMPARs (in *white*) were located within 125 nm from the release site, whereas gating was observed throughout the synapse, as observed by others (21,31,32). Finally, the desensitization protocol of Budisantoso et al. (21) was delivered to assess the rate of recovery from desensitization. In these simulations, instead of a square pulse of glutamate, glutamate was released every 1 ms for a duration of 17 ms. As
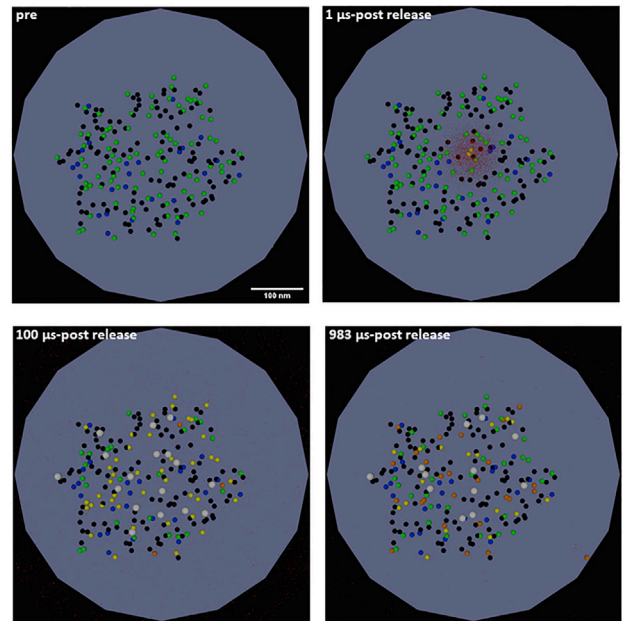
AMPAR

NMDAR   **GluT**

FIGURE 2 Kinetic scheme for AMPAR, NMDAR, and glutamate trans-porters. For AMPAR, the resting state is R_0; C1 and C2 are closed states; O is the open state; D1, D2, D3, D4, and D2_4 are desensitized states. k_1, k_2, β, k_3, k_4, k_5, k_6, k_7, k_8, k_9, and k_{10} are forward rates; k_{-1}, α, k_{-2}, k_{-3}, k_{-4}, k_{-5}, k_{-6}, k_{-7}, k_{-8}, k_{-9}, and k_{-10} are the backward rates. The three-gluta-mate binding and dissociation events are shown. The gray box indicates the kinetic scheme utilized in Heine et al. (4). NMDAR, the resting state is R_0; C1 and C2 are closed states; O is the open state; D is the desensitized state. k_1, k_2, β, and k_3 are forward rates; k_{-1}, α, k_{-2}, and k_{-3} are the backward rates. GluT is resting state T_0; T1 is glutamate bound facing the synaptic cleft, T2 is glutamate transport away from the synapse, T0 is glutamate dissociation. The value of the rate constant is given in Table 1.

the time between the first and second glutamate pulse increased, the number of opened AMPARs recovered from desensitized states increased. After 50 ms, only five receptors could open, and at 100 ms, only 11 entered the open state (Fig. 4, *B and C*), mirroring the exponential curve published by Budisantoso et al. (21). Taken together, these results demonstrate this model can recapit-ulate glutamate transport, the spatiotemporal activation of AMPARs, and the recovery from desensitization as seen by others (30–32).

Once the parameters were validated, AMPARs were as-signed a diffusion coefficient. The average instantaneous diffusion coefficient (D_{inst}) was extracted from a distribu-tion containing 90–95% of slow-moving AMPARs with an average D_{inst} between 0.00001 and 0.01 μm^2/s and 5–10% of fast-moving AMPARs with an average D_{inst} of 0.1 μm^2/s (10,13,15,17). In general, synaptic AMPARs have a D_{inst} ranging from 0.00001 to 0.01 μm^2/s and extrasynaptic AMPARs have a higher average D_{inst} of 0.1 μm^2/s. The distribution and average D_{inst} for AMPARs is shown in Fig. 5, *A and B* and Table 2. These numbers were utilized instead of the most common D_{inst} value of 0.1 μm^2/s, which is not able to capture the fast diffusion for extrasynaptic AMPARs and slow diffusion for synaptic AMPARs (4). For all simulations, the mobility of AMPARs was increased by fivefold for the desensitized states to conform to the values published by Constals et al., intended to mimic AMPAR stargazin dissociation (17). The mean
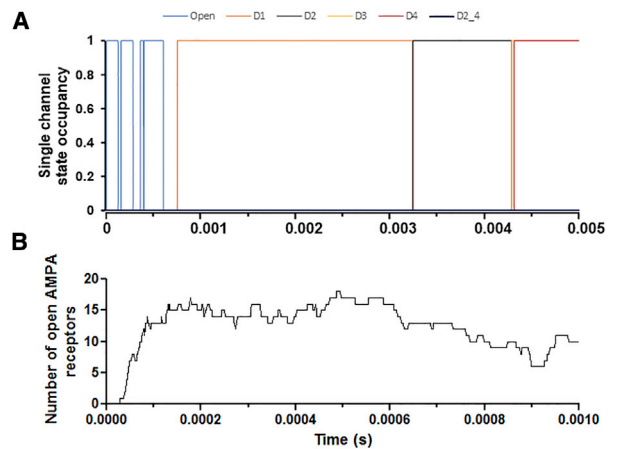
FIGURE 3 AMPAR gating in response to glutamate release. (*A*) Occu-pancy of the kinetic states shown in Fig. 2 for a single AMPAR. A 5 ms long simulation is shown. (*B*) Opening of AMPARs in response to the release of 4000 glutamate molecules. 1 ms of simulation is shown. (*C*) Snapshots of the 1 ms long simulation showing the gating of AMPARs in response to glutamate (in *red*). The color code is as follows: green, closed state; yellow, single- and double-glutamate-bound closed state; white, opened state; and brown, desensitized states. To see this figure in color, go online.

diffusion coefficient of NMDARs and other molecules was set to 0.00001 μm^2/s.

The role of AMPAR diffusion in PPD was examined utiliz-ing a 60 ms interpulse interval. The number of opened and de-sensitized AMPARs was recorded in control conditions or in conditions that the AMPARs were immobilized. The immobi-lization of AMPARs was achieved by setting the D_{inst} of all AMPARs to 0.00001 μm^2/s (Fig. 5 *C*; Table 2). Immobilizing AMPARs failed to decrease the number of open AMPARs in response to the second glutamate pulse (Fig. 5, *D–F*; Videos S2 and S3). Rather than promoting more PPD, immobilizing
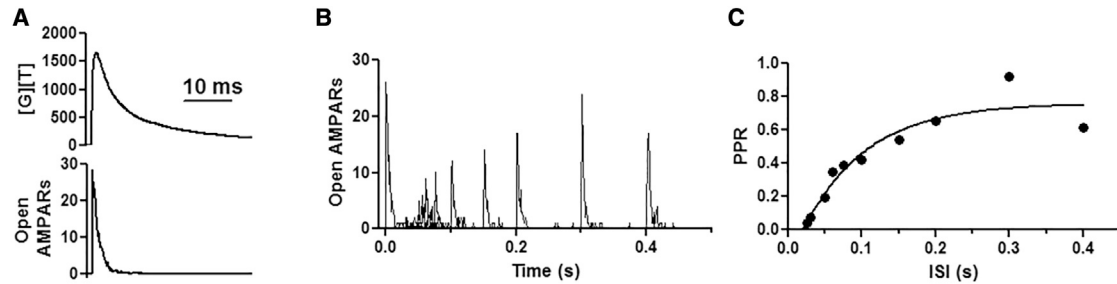
FIGURE 4 Validation of the model. (*A*) (*top*) Binding of glutamate [G] with the transporters [T]. [G][T] symbolizes complex formation. (*Bottom*) Number of open AMPARs in response to glutamate release. (*B*) Single-simulation runs demonstrating the recovery from desensitization, and (*C*) fit of the data shown as paired-pulse ratio (PPR). The calculations were made with respect to the peak of the response.

AMPARs resulted in less PPD, shown as paired-pulse ratio (PPR) (PPR mobile, 0.78 ± 0.18; immobile, 0.93 ± 0.18; $n = 20$; **$p = 0.0095$ by unpaired t-test), which contradicts the diffusion hypothesis (4,17,19,33–36). A different AMPAR gating kinetic scheme was used to compare the effects of changing the desensitization rates on the response with paired-pulse stimulation, as published in (4,23) (Fig. 2 *gray box*; Table 1). Immobilizing AMPARs once again failed to decrease the number of open AMPARs in response to the second glutamate pulse (Fig. 5 *G*), and less PPD was observed (PPR mobile, 0.82 ± 0.11; immobile, 0.95 ± 0.23; $n = 10$; *$p = 0.048137$ by one-tailed unpaired t-test), Moreover, when the original data presented in Fig. 1 of Heine et al. (4) was reanalyzed back in 2011, it revealed no change in PPR and when the neurons were matched by age, a trend of an increase in PPR after cross-linking the AMPARs was observed and communicated to all authors (PPR control, $n = 17$, 0.89 ± 0.32 and PPR X-Link, $n = 12$, 1.19 ± 0.79; $p = 0.58$ by Mann-Whitney test (4)). The only role for mobility was observed when an unphysiological large number of extrasynaptic AMPARs (a ratio of 3:1 extrasynaptic/synaptic) was combined with a different kinetic scheme (Fig. 5 *H*; Table 2, eighth column). Under those conditions, the immobilization of AMPARs increased the amounts of PPD in response to the second glutamate pulse (PPR mobile, 0.98 ± 0.26; immobile 0.77 ± 0.18; $n = 10$; *$p = 0.032256$ by one-tailed unpaired t-test).

Next, the effects of increasing the number of mobile AMPARs was evaluated. To increase the mobility of AMPARs, the ratio of extrasynaptic/synaptic AMPARs was changed from 17.2:1 to 1.1:1 (Fig. 6, *A and B*; Table 2, third to seventh column). In vivo, a ratio of 10 synaptic/one extrasynaptic AMPAR is observed (11–13,37). Increasing the number of mobile extrasynaptic AMPARs from 5 to 80 failed to alter the number of open AMPARs in response to the paired-pulse protocol and, instead, produced an overall increase in the number of desensitized AMPARs (Fig. 6, *D and E*; (PPR 5) $n = 10$, 0.78 ± 0.14; (PPR 10) $n = 10$, 0.83 ± 0.19; (PPR 20) $n = 9$, 0.74 ± 0.10; (PPR 40) $n = 9$, 0.87 ± 0.19; (PPR 80) $n = 10$, 0.89 ± 0.19, $p = 0.29$ by one-way ANOVA; $F (4, 43) = 1.28$; Videos S4, S5, S6, S7, and S8). The condition with

80 extrasynaptic AMPARs conforms to the commonly used value of average D_{inst} of 0.1 $\mu m^2/s$ (4,15,19,35,36,38).

The role of AMPAR mobility in PPD has only been described in cultured neurons without astrocytes. Furthermore, the majority of the experiments testing the role of AMPAR cross-linking were performed using an iontophoresis pipette filled with 150 mM sodium glutamate (4). Therefore, the role of glutamate diffusion and AMPAR mobility was examined in two ways: 1) by altering the number of glutamate molecules released at the synaptic cleft and 2) by altering the density of glutamate transporters (Fig. 7 *A*). Increasing or decreasing the number of glutamate molecules released into the synaptic cleft did not reveal a role for AMPAR mobility in PPD (Fig. 7 *B*). An inverse correlation was observed between the PPR and the number of glutamate molecules, with less PPD when fewer glutamate molecules were released and more PPD with increasing amounts of glutamate. Changing the number of glutamate transporters also did not reveal a role for AMPAR mobility in helping the synapse recover faster from PPD. An increase in the PPR was observed when no glia were present (graphed at 100,000 transporters/μm^2), but decreasing the number of transporters had no effect on the PPR.

Recently, it has been suggested that AMPAR nanodomains could function independently, and that these nanodomains "help" synapses recover from PPD by replacing nondesensitized AMPARs from one nanodomain with AMPARs from the stimulated nanodomain (35,36). To test the idea of AMPAR exchange between nanodomains, glutamate was released into two zones within the synapse, separated by 190 nm (Fig. 8). The two areas in the synapse are labeled as nanodomain 1, which contains 41 AMPARs (*red circle*), and nanodomain 2, which contains 27 AMPARs (*yellow circle*) (Fig. 8). Releasing glutamate onto nanodomain 1 (*left image*, same release) activated most of the receptors within the nanodomain, but the release of glutamate 50 ms later opened a similar number of total AMPARs on both nanodomain 1 and nanodomain 2 (*top row*). Whereas nanodomain 1 started with 41 AMPARs, it lost five AMPARs within the 50 ms interval. Next, the random release condition was tested by releasing glutamate into in nanodomain 1 followed by release in nanodomain 2. Under these conditions, the second
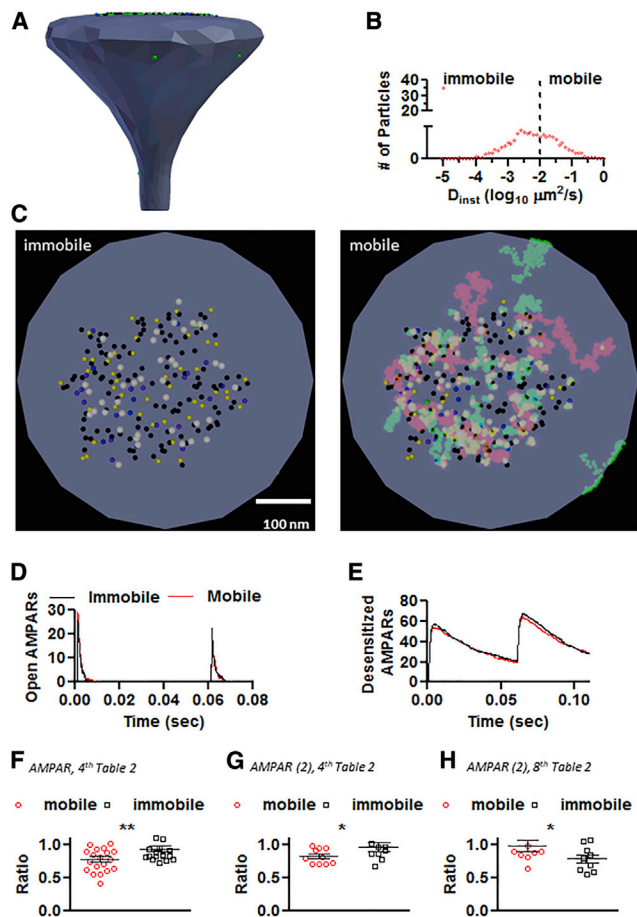
FIGURE 5 Surface AMPAR diffusion and PPD of the CellBlender-based glutamatergic synapse in response to AMPAR immobilization. (A) The rendered postsynaptic spine. (B) Distribution of diffusion coefficient for the simulated conditions. For the immobile condition, all particles have an average value of D_{inst} of 1×10^{-5} $\mu m^2/s$. (C) Maximal projection of 60 ms of simulation. The immobile condition simulates AMPARs cross-linking. The colors follow the kinetic color scheme. The mobile condition uses the values extracted from Nair et al. (10). (D) Number of open AM-PARs in response to a 60 ms paired-pulse stimulation and PPD ratio (F), **$p = 0.0095$. (E) Number of desensitized AMPARs for the simulation shown in (D). (G) PPD ratio for the conditions shown in the fourth column of Table 2, using the AMPAR (2) kinetic scheme (gray box) Fig. 2, *$p = 0.048137$. (H) PPD ratio for the conditions shown in the eighth column of Table 2, using the AMPAR (2) kinetic scheme (gray box) Fig. 2, *$p = 0.032256$. To see this figure in color, go online.

release activated a lower number of AMPARs, and again, no role for AMPAR mobility was observed. Whereas nanodomain 2 started with 27 AMPARs, it gained one AMPAR within the 50 ms interval, suggesting that within 50 ms the AMPAR exchange rate between nanodomains is insufficient to impact the number of open AMPARs during paired-pulse stimulation.

DISCUSSION

The diffusion hypothesis requires the following to be true: 1) the average D_{inst} of AMPARs must be ≥ 0.1 $\mu m^2/s$, and

TABLE 2 Average values of instantaneous diffusion coefficient

Location	Average D_{inst} ($\mu m^3/s$)	Number of receptors					
Extrasynaptic	0.1	5	10	20	40	80	80
PSD	0.01	19	19	19	19	19	0
PSD	0.0005	38	38	38	38	38	0
PSD	0.00001	29	29	29	29	29	29

2) there must be a sufficiently large pool of fast-moving extrasynaptic receptors. Whereas the older models used these parameters and were able to reproduce the biological data, there are significant differences between the older models and the model presented here (4). This model uses morphologically realistic parameters rather than a planar membrane (24–26). Furthermore, the number of synaptic AMPARs used in this model was obtained from experiments in which individual particles were counted from a freeze-fractured image (11,21). This model also uses 4000 glutamate molecules instead of 10,000 (21,30), and the values of AMPAR diffusion coefficients were obtained from recent publications (10,13,15,17) instead of the previously used average D_{inst}-value of 0.1 $\mu m^2/s$ (4,19,35,36,39). Finally, a different kinetic scheme was used in this study to capture the opening, closing, and desensitization of endogenous AMPARs (21). Therefore, the model presented here is an improved representation of the physiology at excitatory synapses.

The original diffusion hypothesis was modified in 2013 to address concerns with the experimental data (10). That modification proposed that AMPARs are organized into nanodomains and that each synapse contains several nanodomains. It was also suggested that nanodomains could operate independently and that this nanodomain organization helps synapses recover from PPD through the sharing of nondesensitized AMPARs from nonstimulated to stimulated nanodomains. In this study, this idea was tested, and several differences were found. First, Compans et al. (36) proposed that AMPAR activation is restricted to 125 nm from the site of glutamate release, whereas these simulations demonstrate that many of the open AMPARs are closer to the release site; however, AMPAR opening occurs even at extrasynaptic sites (>200 nm). Furthermore, when glutamate was released at the center of the synapse, it gated over 95% of synaptic AMPARs, regardless of their distribution across the PSD (Fig. 3) (10,17,35,39). The simulations also show that most AMPARs are not able to travel distances greater than 300 nm in under 60 ms (15), even when the mobility of the desensitized state was accelerated to the constant values published by Constals et al. (17). In fact, in the example shown in Fig. 6, using 10 extrasynaptic AMPARs to simulate the most physiological conditions, only three AMPARs reached the synaptic cleft and, of these, only one became desensitized as it entered the synaptic cleft. Furthermore, none of the synaptic AMPARs left the synapse. It is important to note that these simulations do not contradict the role of nanodomain AMPAR organization in regulating changes
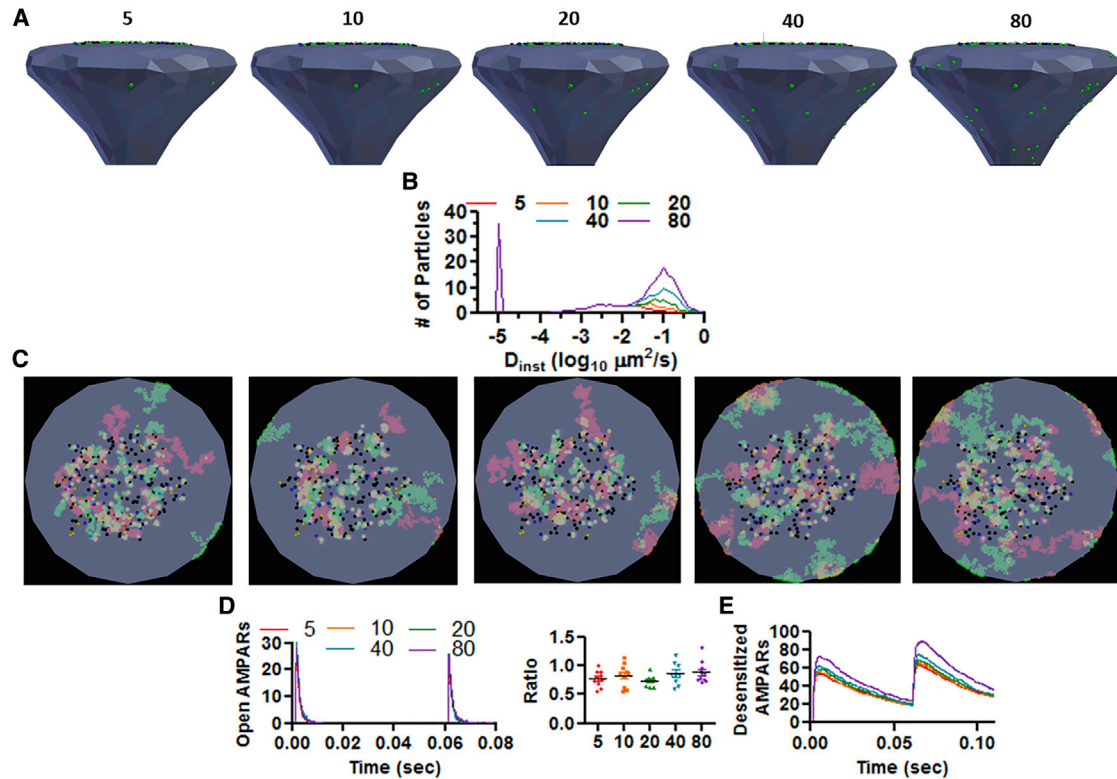
FIGURE 6 Surface AMPAR diffusion and PPD of the CellBlender-based glutamatergic synapse in response to an increase in mobile pool of AMPARs. (*A*) Rendered postsynaptic spine showing number of extrasynaptic AMPARs on top (*green dots*). (*B*) Distribution of diffusion coefficient for the various simulated conditions. (*C*) Maximal projection of 60 ms of simulation showing the extent of diffusion for AMPARs in different activation states. (*D*) Number of open AMPARs in response to a 60 ms paired-pulse stimulation; PPD ratio shown on right. There is no statistical difference in PPD across conditions. (*E*) Number of desensitized AMPARs for the simulation shown in (*D*). To see this figure in color, go online.

in synaptic strength after the induction of synaptic plasticity (40,41). The results only indicate that when physiological amounts of glutamate are released, most (if not all) AMPARs will be gated, irrespective of their location.

There are several possible explanations as to when or if the diffusion of AMPARs may play a role during PPD. One possibility is that this effect is primarily engaged when AMPARs are activated using glutamate uncaging or iontophoresis. In experiments using the glutamate iontophoresis approach, Heine et al. (4) demonstrated that AMPAR diffusion played a role in paired-pulse stimulation only in neurons that diffusely expressed the GluA1 subunit of AMPARs; however, when the GluA1 appeared clustered, as within dendritic spines, then no effect for AMPAR diffusion was observed. This indicates that if glutamate activates a small enough area of the dendrite, then diffusion can play its proposed role, but within dendritic spines, it does not appear to play a role. The findings presented here are further supported by Penn et al., who demonstrated that cross-linking AMPARs in organotypic slices does not alter the paired-pulse response (42), and by the results of Budisantoso et al., who proposed that if AMPAR diffusional exchange occurred between glomerular synapses, then most of the AMPARs would enter the desensitized state and not play a

role in PPD (21). Alternatively, it may be that when using antibodies to induce the cross-linking of AMPARs, rates of desensitization are affected, as is the case of antibodies against NMDARs(43).

CONCLUSIONS

Collectively, these findings show that AMPAR diffusion may play little or no role during paired-pulse stimulation of excitatory synapses, and it seems that AMPAR surface diffusion is more important for other physiological processes, such as synapse development, AMPAR recycling, and AMPAR recruitment after the induction of synaptic plasticity.
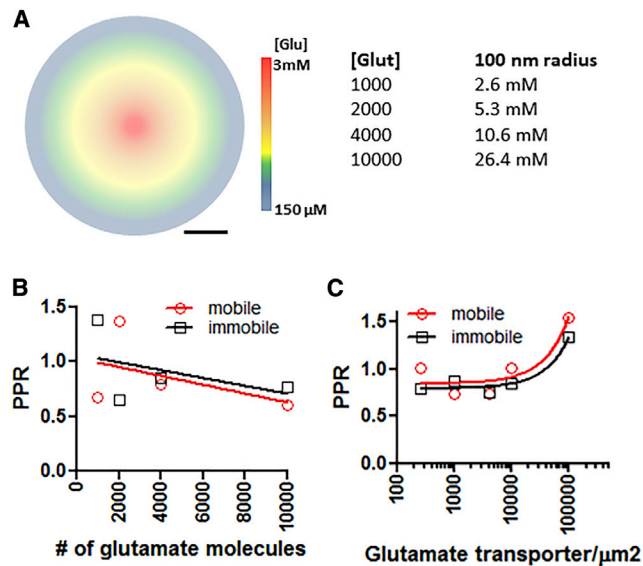
SUPPORTING MATERIAL

Supporting material can be found online at https://doi.org/10.1016/j.bpj.2021.06.026.

FIGURE 7 Effects of changing the rates of glutamate transport from the synapse. (*A*) Cartoon representing the different concentrations of glutamate postrelease. [Glut] shows the number of glutamate molecules released and its calculated concentration within a 100 nm radius. (*B*) The effects of the number of released glutamate molecules on the PPR. (*C*) Effects of changing the density of glutamate transporters and AMPAR mobility on the PPR. To see this figure in color, go online.

REFERENCES

1. Stevens, C. F. 2003. Neurotransmitter release at central synapses. *Neuron.* 40:381–388.

2. Acuna, C., Q. Guo, …, T. C. Südhof. 2014. Microsecond dissection of neurotransmitter release: SNARE-complex assembly dictates speed and Ca^{2+} sensitivity. *Neuron.* 82:1088–1100.

3. Jackman, S. L., and W. G. Regehr. 2017. The mechanisms and functions of synaptic facilitation. *Neuron.* 94:447–464.

4. Heine, M., L. Groc, …, D. Choquet. 2008. Surface mobility of postsynaptic AMPARs tunes synaptic transmission. *Science.* 320:201–205.

5. Inavalli, V. V. G. K., M. O. Lenz, …, U. V. Nägerl. 2019. A super-resolution platform for correlative live single-molecule imaging and STED microscopy. *Nat. Methods.* 16:1263–1268.

6. Groc, L., M. Heine, …, D. Choquet. 2004. Differential activity-dependent regulation of the lateral mobilities of AMPA and NMDA receptors. *Nat. Neurosci.* 7:695–696.

7. Saglietti, L., C. Dequidt, …, M. Passafaro. 2007. Extracellular interactions between GluR2 and N-cadherin in spine regulation. *Neuron.* 54:461–477.

8. Tardin, C., L. Cognet, …, D. Choquet. 2003. Direct imaging of lateral movements of AMPA receptors inside synapses. *EMBO J.* 22:4656–4665.

9. Triller, A., and D. Choquet. 2005. Surface trafficking of receptors between synaptic and extrasynaptic membranes: and yet they do move! *Trends Neurosci.* 28:133–139.

10. Nair, D., E. Hosy, …, J.-B. Sibarita. 2013. Super-resolution imaging reveals that AMPA receptors inside synapses are dynamically organized in nanodomains regulated by PSD95. *J. Neurosci.* 33:13204–13224.
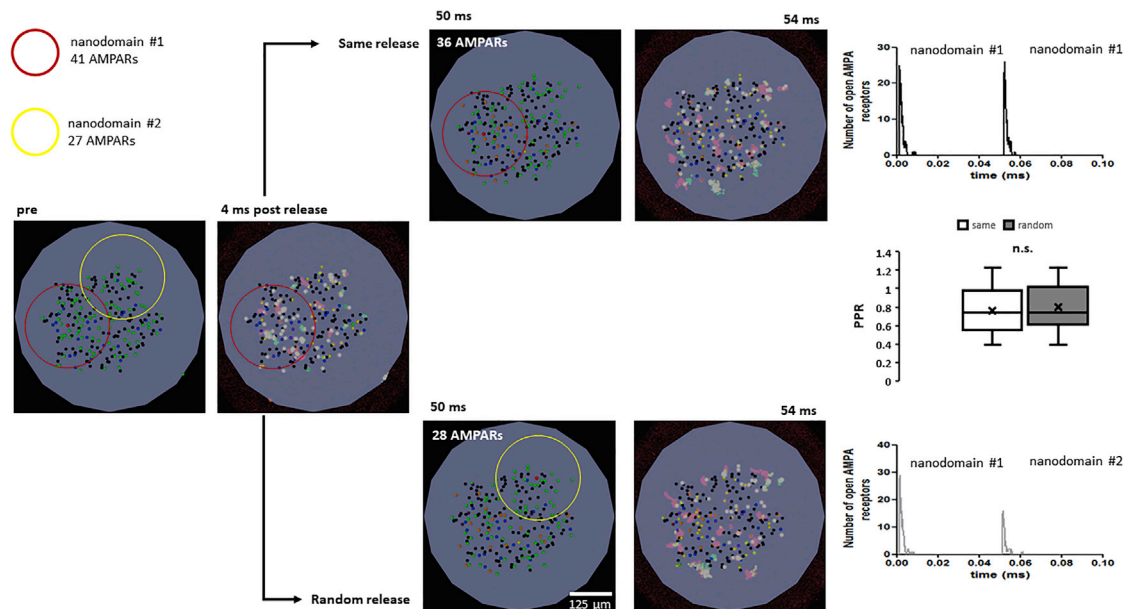
FIGURE 8 Effects of glutamate release at different nanodomains. The red circle highlights the area of nanodomain 1 containing 41 AMPARs. The yellow circle highlights the area of nanodomain 1 containing 27 AMPARs. "pre" shows the image before glutamate release; the maximal projection image of 4 ms after glutamate release is shown to the right. "Same release" shows a snapshot of the state of the synapse at 50 ms after glutamate release; the maximal projection image of 4 ms after glutamate release is at the center of the red circle. (*Top right*) Number of open AMPARs under the same release condition. "Random release" shows a snapshot of the state of the synapse at 50 ms after glutamate release; the maximal projection image of 4 ms after glutamate release is at the center of the yellow circle. The number of open AMPARs under the random release condition is shown. No difference in PPR is observed in either condition (*middle graph*). To see this figure in color, go online.

11. Shinohara, Y., and H. Hirase. 2009. Size and receptor density of gluta-matergic synapses: a viewpoint from left-right asymmetry of CA3–CA1 connections. *Front. Neuroanat.* 3:10.

12. Matsuzaki, M., G. C. Ellis-Davies, …, H. Kasai. 2001. Dendritic spine geometry is critical for AMPA receptor expression in hippocampal CA1 pyramidal neurons. *Nat. Neurosci.* 4:1086–1092.

13. Lee, S. H., C. Jin, …, P. R. Selvin. 2017. Super-resolution imaging of synaptic and Extra-synaptic AMPA receptors with different-sized fluorescent probes. *eLife.* 6:e27744.

14. Li, T. P., and T. A. Blanpied. 2016. Control of transmembrane protein diffusion within the postsynaptic density assessed by simultaneous single-molecule tracking and localization microscopy. *Front. Synaptic Neurosci.* 8:19.

15. Delgado, J. Y., and P. R. Selvin. 2018. A revised view on the role of surface AMPAR mobility in tuning synaptic transmission: limitations, tools, and alternative views. *Front. Synaptic Neurosci.* 10:21.

16. Li, T. P., Y. Song, …, S. Raghavachari. 2016. Protein crowding within the postsynaptic density can impede the escape of membrane proteins. *J. Neurosci.* 36:4276–4295.

17. Constals, A., A. C. Penn, …, D. Choquet. 2015. Glutamate-induced AMPA receptor desensitization increases their mobility and modulates short-term plasticity through unbinding from Stargazin. *Neuron.* 85:787–803.

18. Groc, L., M. Lafourcade, …, L. Cognet. 2007. Surface trafficking of neurotransmitter receptor: comparison between single-molecule/quantum dot strategies. *J. Neurosci.* 27:12433–12437.

19. Czöndör, K., M. Mondin, …, O. R. Thoumine. 2012. Unified quantitative model of AMPA receptor trafficking at synapses. *Proc. Natl. Acad. Sci. USA.* 109:3522–3527.

20. Gupta, S., J. Czech, …, J. R. Faeder. 2018. Spatial stochastic modeling with MCell and CellBlender. *arXiv*, arXiv:1810.00499 [q-bio.QM] https://arxiv.org/abs/1810.00499.

21. Budisantoso, T., K. Matsui, …, R. Shigemoto. 2012. Mechanisms underlying signal filtering at a multisynapse contact. *J. Neurosci.* 32:2357–2376.

22. Lester, R. A., and C. E. Jahr. 1992. NMDA channel behavior depends on agonist affinity. *J. Neurosci.* 12:635–643.

23. Jonas, P., G. Major, and B. Sakmann. 1993. Quantal components of unitary EPSCs at the mossy fibre synapse on CA3 pyramidal cells of rat hippocampus. *J. Physiol.* 472:615–663.

24. Arellano, J. I., R. Benavides-Piccione, …, R. Yuste. 2007. Ultrastructure of dendritic spines: correlation between synaptic and spine morphologies. *Front. Neurosci.* 1:131–143.

25. Harris, K. M., F. E. Jensen, and B. Tsao. 1992. Three-dimensional structure of dendritic spines and synapses in rat hippocampus (CA1) at postnatal day 15 and adult ages: implications for the maturation of synaptic physiology and long-term potentiation. *J. Neurosci.* 12:2685–2705.

26. Harris, K. M., and J. K. Stevens. 1989. Dendritic spines of CA 1 pyramidal cells in the rat hippocampus: serial electron microscopy with reference to their biophysical characteristics. *J. Neurosci.* 9:2982–2997.

27. Lehre, K. P., and N. C. Danbolt. 1998. The number of glutamate transporter subtype molecules at glutamatergic synapses: chemical and stereological quantification in young adult rat brain. *J. Neurosci.* 18:8751–8757.

28. Holmseth, S., Y. Dehnes, …, N. C. Danbolt. 2012. The density of EAAC1 (EAAT3) glutamate transporters expressed by neurons in the mammalian CNS. *J. Neurosci.* 32:6000–6013.

29. Franks, K. M., T. M. Bartol, Jr., and T. J. Sejnowski. 2002. A Monte Carlo model reveals independent signaling at central glutamatergic synapses. *Biophys. J.* 83:2333–2348.

30. Diamond, J. S. 2005. Deriving the glutamate clearance time course from transporter currents in CA1 hippocampal astrocytes: transmitter uptake gets faster during development. *J. Neurosci.* 25:2906–2916.

31. Raghavachari, S., and J. E. Lisman. 2004. Properties of quantal transmission at CA1 synapses. *J. Neurophysiol.* 92:2456–2467.

32. Tarusawa, E., K. Matsui, …, R. Shigemoto. 2009. Input-specific intrasynaptic arrangements of ionotropic glutamate receptors and their impact on postsynaptic responses. *J. Neurosci.* 29:12896–12908.

33. Frischknecht, R., M. Heine, …, E. D. Gundelfinger. 2009. Brain extracellular matrix affects AMPA receptor lateral mobility and short-term synaptic plasticity. *Nat. Neurosci.* 12:897–904.

34. Gundelfinger, E. D., R. Frischknecht, …, M. Heine. 2010. Converting juvenile into adult plasticity: a role for the brain's extracellular matrix. *Eur. J. Neurosci.* 31:2156–2165.

35. Groc, L., and D. Choquet. 2020. Linking glutamate receptor movements and synapse function. *Science.* 368:eaay4631.

36. Compans, B., D. Choquet, and E. Hosy. 2016. Review on the role of AMPA receptor nano-organization and dynamic in the properties of synaptic transmission. *Neurophotonics.* 3:041811.

37. Kneussel, M., and T. J. Hausrat. 2016. Postsynaptic neurotransmitter receptor reserve pools for synaptic potentiation. *Trends Neurosci.* 39:170–182.

38. Pandya, N. J., C. Seeger, …, A. B. Smit. 2018. Noelin1 affects lateral mobility of synaptic AMPA receptors. *Cell Rep.* 24:1218–1230.

39. Choquet, D., and E. Hosy. 2020. AMPA receptor nanoscale dynamic organization and synaptic plasticities. *Curr. Opin. Neurobiol.* 63:137–145.

40. Tang, A.-H., H. Chen, …, T. A. Blanpied. 2016. A trans-synaptic nanocolumn aligns neurotransmitter release to receptors. *Nature.* 536:210–214.

41. MacGillavry, H. D., Y. Song, …, T. A. Blanpied. 2013. Nanoscale scaffolding domains within the postsynaptic density concentrate synaptic AMPA receptors. *Neuron.* 78:615–622.

42. Penn, A. C., C. L. Zhang, …, D. Choquet. 2017. Hippocampal LTP and contextual learning require surface diffusion of AMPA receptors. *Nature.* 549:384–388.

43. Chan, K., J. Nestor, …, L. P. Wollmuth. 2020. Lupus autoantibodies act as positive allosteric modulators at GluN2A-containing NMDA receptors and impair spatial memory. *Nat. Commun.* 11:1403.